Contrib Mineral Petrol (2009) 157:111–126
DOI 10.1007/s00410-008-0323-z

ORIGINAL PAPER

A pre-edge analysis of Mn K-edge XANES spectra to help determine the speciation of manganese in minerals and glasses

E. Chalmin · F. Farges · G. E. Brown Jr

Received: 21 February 2008 / Accepted: 23 June 2008 / Published online: 22 July 2008

Abstract High-resolution manganese K-edge X-ray absorption near edge structure spectra were collected on a set of 40 Mn-bearing minerals. The pre-edge feature information (position, area) was investigated to extract as much as possible quantitative valence and symmetry information for manganese in various "test" and "unknown" minerals and glasses. The samples present a range of manganese symmetry environments (tetrahedral, square planar, octahedral, and cubic) and valences (II to VII). The extraction of the pre-edge information is based on a previous multiple scattering and multiplet calculations for model compounds. Using the method described in this study, a robust estimation of the manganese valence could be obtained from the pre-edge region at 5% accuracy level. This method applied to 20 "test" compounds (such as hausmannite and rancieite) and to 15 "unknown" compounds (such as axinite and birnessite) provides a quantitative estimate of the average valence of manganese in complex minerals and silicate glasses.

Keywords Manganese · Valence · Symmetry · Mineral · Glass · XANES pre-edge

Communicated by J. Hoefs.

Electronic supplementary material The online version of this article (doi:10.1007/s00410-008-0323-z) contains supplementary material, which is available to authorized users.

E. Chalmin (✉)
European Synchrotron Radiation Facility,
38043 Grenoble, France
e-mail: chalmin@esrf.fr

F. Farges
Unité Minéralogie-Pétrologie, Muséum National d'Histoire Naturelle and CNRS UMR 7160, Paris, France

F. Farges · G. E. Brown Jr
Department of Geological and Environmental Sciences, Stanford University, Stanford, CA 94305-2115, USA

G. E. Brown Jr
Stanford Synchrotron Radiation Laboratory, SLAC,
2575 Sand Hill Road, MS 69, Menlo Park, CA 94025, USA

Introduction

Manganese is the third most abundant transition element in Earth materials, following iron and titanium (Greenwood and Earnshaw 1984). Manganese occurs in a variety of valences depending on formation conditions. For example, trivalent and tetravalent forms of manganese are observed in Earth materials derived from hydrothermal fluids and supergene environments (see Post 1999). On the other hand, manganese is dominantly divalent in mafic and ultramafic igneous rocks formed under more reducing conditions but also in some metamorphic rocks (Petrie 1999). However, in some Mn-containing minerals, several valences of manganese can coexist as in hausmannite ($(Mn(II)Mn(III)_2O_4$; Baron et al. 1998) or in birnessite ($\sim (Na,Ca,K)_x(Mn(IV),Mn(III))_{2-x}O_4$ $1.5(H_2O)$; see Drits et al. 2002; Manceau et al. 2002). In the latter, charge compensation around manganese occurs because of other cationic substitutions (often alkalis, alkali-earths, iron, and/or hydrogen), which are not always straightforward to evaluate (in the case of protons, for instance). Therefore, the prediction of the valence of manganese is not always straightforward based on the chemistry alone, particularly in hydrous minerals. Direct measurements of the actual manganese valence are then required to fully validate these charge compensation assumptions. On the other hand, the concept of valence is more and more challenged by

physicists (see de Groot 2001; Tromp et al. 2007). Ab initio charge transfer calculations show that the effective charge for many transition elements can vary significantly for a given valence (see Farges 2005). However, this last study showed, based on self-consistent calculations, that the deviation from the formal valence of manganese in various oxides and silicate rock-forming minerals is negligible for most petrological and mineralogical studies.

Several spectroscopic methods, including electron paramagnetic resonance (see Calas 1984), electron energy loss and X-ray photoemission spectroscopies (see Garvie et al. 1994), optical absorption spectroscopy (see Manning 1970, 1973; Burns 1993), and X-ray absorption fine structure (XAFS) spectroscopy are sensitive to manganese valences. Past XAFS studies have extracted manganese valence information from the extended XAFS region through crystal chemical interpretations of EXAFS-derived Mn–O distances (see, e.g., Manceau et al. 1992b; Marcus et al. 2004). More often, the valence of manganese is estimated from the Mn K-edge position (see among others, Schulze et al. 1995; Manceau et al. 1992a, 2000; Bargar et al. 2000; Ressler et al. 2000; McKeown and Post 2001; Guest et al. 2002; McKeown et al. 2003; Farges 2005; Tebo et al. 2004) and also in patrimonial artifacts (Reiche et al. 2001; Quartieri et al. 2002; Farges et al. 2005). Qualitatively, the Mn K-edge shifts toward higher energies with increasing manganese valence, as for most other transition elements. This is because the X-ray absorption near edge structure (XANES) region involves bound-state electronic transitions from deep core levels to valence levels. The energy positions of near-edge features are particularly sensitive to changes in shielding of nuclear charge provided by valence electrons. In practice, either the first inflexion point of the Mn K-edge or the edge crest are chosen as a measure of the valence of manganese in a sample by Mn K-edge XANES spectroscopy. Unfortunately, this method has been proven to conduct to up to 90% misestimating in the actual manganese valence (Farges 2005). This is due to the possibility of constructive and destructive interferences between atomic absorption (sensitive to valence) with multiple-scattering features from distant neighbors (more sensitive instead to the local geometry).

Then, more attention has been paid to the pre-edge feature at the K-edge for determining the valence of valence-sensitive elements (see, among others, Belli et al. 1980; Westre et al. 1997; Nietubyc et al. 2001; Visser et al. 2001; Wilke et al. 2001; Glatzel et al. 2004). In the case of manganese, the pre-edge feature is located $\sim$15–20 eV before the main K-edge crest and is linked to crystal field transition (from the core 1s levels to the empty 3d levels, more or less 4p hybridized by the manganese ligands). At the Mn K-edge, the pre-edge region is much less influenced by the medium- and long-range structure as compared to the edge jump or edge crest regions. However, only a few studies have focused on the pre-edge region (among them, Manceau et al. 1992a; Quartieri et al. 2002), but none so far could provide an accurate and reliable estimation of manganese valence (see de Groot 2001; Visser et al. 2001; Nietubyc et al. 2001; Gilbert et al. 2003; Glatzel et al. 2004; Farges 2005; Glatzel and Bergmann 2005; Glatzel et al. 2005).

In this study, we present the results of a high-resolution XANES spectroscopy study obtained for 40 Mn-bearing model compounds, including numerous natural and some synthetic oxides and silicates containing manganese in different valences (II–VII) and with various symmetries (octahedral, square planar, cubic, or tetrahedral). A short description of the method of calibration using the Mn pre-edge XANES spectra of reference compounds is given. And then, the XANES pre-edge spectra of additional 35 compounds were used as test cases to determine how well this approach works and as "unknowns" (such as rock-forming minerals, glasses, soils-based oxyhydroxides) to determine the manganese speciation (valence and symmetry) of more complex minerals and glasses.

Experimental method

XAFS data collection and normalization

Mn K-edge XANES spectra for model compounds were collected on beamline 11-2 at SSRL (Stanford, USA) using the SPEAR2 storage ring. XANES data were collected under high resolution conditions (2σ $\sim$1.3 eV) using a Si(220) double-crystal monochromator and 0.3 mm vertical height for the slits before and after the monochromator. The energy reproducibility of the monochromator was better than 0.03 eV after 2 days of data collection (tested by recording regularly the spectrum of $KMnO_4$). Pre-edge features were collected using 0.1 eV steps whereas the main edge crest was collected with 0.3 eV steps to 300 eV above the absorption edge. The XANES spectra were usually collected in both the transmission and fluorescence modes with the sample at 90° to the incident X-ray beam to minimize self-absorption effects, following Tröger et al. (1992). When present (as in MnO and Mn_2O_3 in the fluorescence mode), self-absorption effects were taken into account using the FLUO computer code (Haskel 1999). The compositional information required for these corrections was obtained thanks to particle induced X-ray emission (PIXE) (2MV tandem accelerator AGLAE facility) analysis. Samples of MnO, MnOH, $MnCO_3$, Mn_2O_3, MnOOH, and the MnO_2 polymorphs pyrolusite and

ramsdellite were studied in detail to check for the accuracy of the FLUO self-absorption corrections. The self-absorption-corrected spectra were found to be close enough to those collected simultaneously in the transmission mode, including the pre-edge region (despite discrepancies were found, but without significant impact on the pre-edge feature). Finally, for one-third of the samples, spectra were collected two to four times within a 2 years interval to check for spectral reproducibility and chemical stability.

Data extraction and simulation were performed as described in Farges (2005). Briefly, the XANES spectra were normalized in absorbance using standard methods (a combination of polynomial and splines as available in the XAFS package; Winterer 1997). Then, the pre-edge region was extracted from the normalized XANES spectra and modeled using a series of pseudo-Voigt functions (sum of Gaussian and Lorentzian functions) of fixed width (1.3 eV) and of fixed Gaussian percent (45%; Farges 2005), to minimize the number of variable parameters. For each sample, the pre-edge centroid is calculated from the average position of the pseudo-Voigt functions, weighted by their respective integrated areas, after subtraction of baseline continuum. The total integrated area is the sum of the individual integrated areas. The values for the centroid presented in the tables are given with ±0.02 eV and for the integrated area with ±5%. This accuracy level enables to estimate the reproducibility of the pre-edge extraction method.

Model compounds

Table 1 lists the crystalline model compounds used in this study and summarizes the mean centroid position and integrated area obtained after extraction of the pre-edge for the Mn(II) to the Mn(VII) in various symmetry environments (octahedral, tetrahedral, cubic). Manganosite (MnO) proved to be stable under the incident X-ray beam and no trace of oxidation was observed on the sample, in contrast to $KMnO_4$ which showed a relatively quick (within 2 h) but partial (~30%) reduction of Mn(VII) to Mn(IV). All others minerals were single crystals. Commercially available samples of "MnO", "Mn_2O_3", and "MnO_2" in powdered form were obtained from Alfa Inc. and were compared with natural equivalents (manganosite, bixbyite, and pyrolusite/ramsdellite/akhtenskite, respectively). All samples were finely ground and either deposited on Millipore membranes (using either water, acetone or alcohol, depending on the sample solubility) or diluted in boron nitride or cellulose to achieve one to two absorption lengths in transmission at the Mn K-edge. Consequently, no polarization effects were detectable. All of these samples were previously well characterized with other methods (especially the Mn(IV)-rich ones because of their potential complexity), such as X-ray diffraction (XRD), PIXE, or transmission electron microscopy (TEM).

For divalent to the heptavalent compounds, the number of modeled transitions is given in the Table 1, referred to our method (Farges 2005).

Table 1 Summarize of the pre-edge information for the models for Mn(II) to Mn(VII)

Mn environment	Model compounds	Formula	Number of contributions in the pre-edge[a]	Centroid (eV)	Integrated area
Mn(II) O_h	Manganosite	MnO	2	6540.62	0.0745
	Rhodocrosite	$MnCO_3$		6540.66	0.0923
	Pyrochroïte	$Mn(OH)_2$		6540.53	0.1487
	Tephroïte	$Mn_{1.7}Fe_{0.2}Ca_{0.1}SiO_4$		6540.65	0.0907
Mn(II) T_d	Staurolite	$(Mn,Fe)_2Al_9O_7(OH)[SiO_4]_4$	2	6540.59	0.1912
	Jacobsite	$MnFe_2O_4$		6540.65	0.1850
Mn(II) cube	Spessartite	$(Mn,Fe)_3Al_2Si_3O_{12}$	2	6540.66	0.0623
Mn(III) O_h	Manganite	MnOOH	3	6540.98	0.109
	Groutite	MnOOH		6540.98	0.0789
	Bixbyite	Mn_2O_3		6540.81	0.0953
Mn(IV) O_h	Pyrolusite	MnO_2 (tetragonal)	2 + 1 Extra	6541.47	0.0830
	Ramsdellite	MnO_2 (orthorhombic)		6541.59	0.0737
Mn (V) T_d	Ba-Mn chlorapatite	$Ba_5(PO_4)_{2,5}(MnO_4)_{0,5}Cl$	4	6542.05	1.1853
Mn(V) O_h	K_2MnO_4	K_2MnO_4	4	6542.09	0.3173
Mn(VI) T_d	$K_{11}LiMn_4O_{16}$	$K_{11}LiMn_4O_{16}$	5	6542.79	1.3026
Mn(VI) O_h	Ba-manganate	$BaMnO_4$	4	6542.22	1.1034
Mn(VII) T_d	K-permanganate	$KMnO_4$	6	6543.81	2.4299

[a] Both observed and modeled based on theoretical pre-edge calculations (multiple-scattering and multiplets calculations)

Polarized resonant inelastic X-ray scattering (p-RIXS) experiments performed at the Mn K-edge in a single crystal of MnO clearly showed the doublet assigned to the transition of the 1s electron to the 3d crystal-field split states (t_{2g} and e_g, respectively; Dräger et al. 2001). Recent RIXS experiments and multiplets calculations (Glatzel et al. 2004) performed on synthetic manganosite (and other simple manganese oxides) confirm this model. Accordingly, Farges (2005) showed that for the divalent manganese, two transitions (of 1.3 eV width) are required to model the pre-edge.

For trivalent manganese, theoretical calculations (Glatzel and Bergmann 2005; Farges 2005) predicted also three main sets of transitions to model the pre-edge feature of Mn(III)-bearing oxide compounds such as manganite. Further, the influence of Jahn–Teller distortion around Mn(III), variations in charge transfer (the effective charge of manganese in these compounds), variations in local structure and in bulk chemistry do not affect the pre-edge centroid.

Multiplets calculations for a Mn(IV) ion in a site coordinated by six oxygens with O_h (octahedral) point coordination (Glatzel et al. 2004) show that four main sets of transitions are predicted. Ab initio FEFF8.2 calculations show that these four sets of individual transitions can be modeled by three pseudo-Voigt functions (Farges 2005). This model is also experimentally confirmed for all other Mn(IV)-bearing oxides we already investigated.

The two first transitions arise from crystal-field splitting into $t_{2\ g}$ and e_g bands. The third transition is related to extra transition as observed around titanium, iron, and nickel in metal-rich oxides, (Dräger et al. 1988; Heumann et al. 1997; Uozumi et al. 2004). In particular, combined ab initio calculation and p-RIXS analysis on La_2CuO_4 at the Cu K-edge enable to identify a nonlocal effect considered as an off-site 1s-3d dipolar transition (Shukla et al. 2006). In addition, the full-multiplet calculations and the LCAO density-of-state calculation combined to experiment at Ti K-edge lead to an assignment of the origin of the surimposed quadrupolar and dipolar transitions (P-state) as the 3d states of other Ti atoms (Uozumi et al. 2004). Alternatively, Glatzel et al. (2005) attributed those transitions to multiplet effects.

These additional transitions progressively disappear when the extent of metal polymerization decrease, as observed in mononuclear Mn(IV)-bearing complex (e.g., Mn(IV)-acac, acetylacetonate: Glatzel et al. 2004), in diluted Mn(IV) in apatite matrix (90 ppm of Mn, Reiche and Chalmin 2008) or in Cr-bearing spinels (Farges 2008).

The presence of these extra transitions in Mn(IV)-containing compounds explains why previous attempts to extract reliable valence information from the Mn K-edge pre-edge feature were unsuccessful (see Visser et al. 2001). This contribution to the pre-edge feature enhances the pre-edge intensity and can lead to the erroneous conclusion that manganese occupies non-centrosymmetric sites as well as to significant overestimates of the valence of manganese by one or more units. The same conclusions were obtained for both Cr(III) and Cr(IV) (Farges 2008).

As for Mn(II) and Mn(III), the pre-edges for Mn(V), Mn(VI), and Mn(VII) are much more straightforward to analyze than those for Mn(IV). The pre-edge features for pentavalent and hexavalent manganese shows a well-separated doublet when manganese is coordinated by six oxygens with O_h point coordination. These pre-edges are composed by a higher number of electronic transitions than for lower valences of manganese. This could be explained by multiplet approach and is predicted by ab initio calculations. When surrounded by four oxygens with T_d (tetrahedral) geometry (as in Ba-chlorapatite where Mn(V) substitutes for P: Reiche et al. 2001), the manganese pre-edge is relatively intense ($\sim$1/3 of the edge jump), consistent with a loss of centrosymmetry around Mn(V), as observed for other valences of transition elements, including Mn(II) (see, among many others, Farges et al. 1997; Glatzel et al. 2004). The same observation can be made for the XANES pre-edge of Mn(VI)-containing oxides, which also show an intense pre-edge for T_d environment (relative height of 0.7 as compared to the edge jump). When Mn(VI) is surrounded by six nearest-neighbor oxygens with O_h geometry (data from Reiche et al. 2001), a well-resolved doublet is observed. Here again, the centroid of the doublet is the correct measure of the valence state of manganese (and not the maximum as suggested by Reiche et al. 2001). Finally, a fresh sample of potassium permanganate showed one of the highest pre-edge features observed (relative height of 1.1 as compared to the edge jump).

Results and discussion

General trends

Figure 1 summarizes the various pre-edge positions for the different valences of manganese. The model presented in Farges (2005) is validated for higher valence states of manganese (V, VI, and VII). On average, the pre-edges for Mn(V, VI, and VII) are more intense than those for lower valences of manganese, as more 3d levels are empty in these highly oxidized valence states. A systematic shift of the pre-edge position toward higher energy with increasing valence is observed from Mn(II) to Mn(VII). However, this shift is observed when only the Mn K-edge pre-edge features related to crystal field splitting are taken into consideration (and excluding those arising from extra

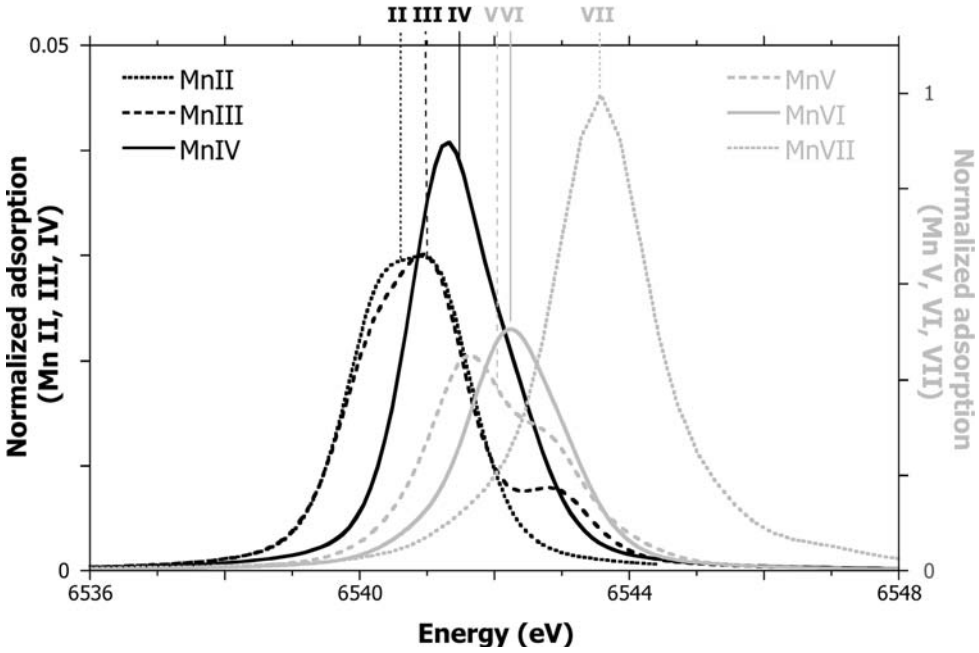

Fig. 1 Shift of the normalized pre-edge feature with Mn-valence, when transitions related to distant manganese are excluded (Sum of pseudo-Voigts contribution for Mn(II): Manganosite, Mn (III): Groutite, Mn(IV): Pyrolusite, Mn(V): Ba-Mn chloroapatite, Mn(VI): $BaMnO_4$, Mn(VII): $KMnO_4$)

pairs). Also, all model compounds investigated show consistent correlations between pre-edge intensity and manganese symmetry environment and between energy of the pre-edge centroid and manganese valence.

Application to known models: the "test" samples

Using a selection of "test" samples, most of which have been well characterized using electron microprobe methods (see mineralogical details of the samples studied in Table 2); we will illustrate how to extract more reliable pre-edge information from the Mn K-edge. The normalized Mn K-edge XANES spectra for the "test" compounds are presented in Fig. 2a, b (data listed in Table 3). Selected modeled pre-edges for these "test" minerals are shown on Fig. 3a.

Examination of the Mn K-edge position is a first qualitative indicator of the valence of manganese (keeping in mind this measurement is not quantitative). This "energy position" can be measured at the half height of the normalized absorbance, i.e., at $\mu = 0.5$. In case of an intermediate energy position (i.e., between divalent and tetravalent), one should model the pre-edge feature with either two or three peaks of fixed width and shape (pseudo-Voigt functions of 1.3 eV 2σ width and 45% Gaussian; see Farges et al. 2004). This approach minimizes the number of free parameters during the modeling and increases the robustness of the model. An additional peak is allowed to vary in position to model potential extra pairs (metal–metal or multiplet-related). If those pairs are not present, this additional feature usually convergences to a near zero height or converge into the baseline components.

Simple oxide: hausmannite

In hausmannite (samples "hausmannite #1" and "hausmannite #2" in Tables 2 and 3 and in Fig. 3a), manganese is distributed over two sites with different coordination numbers and has two valences ($^{[4]}$Mn(II) and $^{[6]}$Mn(III)) (Baron et al. 1998). Accordingly, the pre-edge centroid for both the natural (#1) and synthetic (#2) hausmannite samples is located near 6540.88 eV, which is intermediate between the average centroid for Mn(II) and Mn(III). However, the pre-edge intensity for hausmannite is too high for a centrosymmetric site like O_h (0.2 vs. <0.1), which is related to the presence of tetrahedrally coordinated Mn(II). A theoretical mixture of the pre-edge spectra for NiMn-chromite and manganite model compounds (each of these pre-edges representing, respectively, the contributions arising from tetrahedrally coordinated Mn(II) and octahedrally coordinated Mn(III)) confirms that the 50:50 mechanical mixture between both models has a pre-edge height similar to that for a T_d geometry but a pre-edge centroid position located near 6540.8 eV. Such non-linearities in correlations between valence and pre-edge energy and between coordination number and pre-edge intensity were demonstrated previously for titanium, iron, and chromium (Farges et al. 1996; Wilke et al. 2001; Farges 2008). Finally, the "braunite #1" sample from Langban (Sweden) is confirmed to be a hausmannite (as

Table 2 Mineralogical information for the "test" samples

Sample	Origin	Formula	Valence
Hausmannite #1[a]	N'Chwaning, North Cape, South Africa	Mn_3O_4	II + III
Hausmannite #2	Synthetic (Alfa Inc.)	Mn_3O_4	II + III
Braunite #1[b]	Langban, Varmland, Sweden	$(Mn)Mn_6SiO_{12}$	II + III
Braunite #2	Kajlidongri mine, Madhya Pradesh, India	$(Mn)Mn_6SiO_{12}$	II + III
Franklinite[c]	Franklin, NJ, USA	$Zn_{0,61}Mn_{0,39}(Fe_{1,94}Mn_{0,06})O_4$	II + III
Aurorite	Treasure Hill, Hamilton, NV, USA	$(Mn,Ag,Ca)Mn_3O_7{\cdot}3H_2O$	IV + II
Rancieite	Cassagna Mine, Val Graveglia, Italy	$(Ca,Mn)Mn_4O_9{\cdot}3H_2O$	IV
N'sutite	Nsuta Mine, Tarkwa, Ghana	"δ-MnO_2"	IV + III
Romanechite[c]	Romanèche, Saône et Loire, France	$Ba_{1.1}Ca_{0.1}K_{0.1}Mn_{9.4}Fe_{0.1}Si_{0.4}\ Al_{0.2}O_{20}$	IV + III
Todorokite	DeBely Mine, Death Valley, CA, USA	$(Mn,Ca,Mg)Mn_3O_7{\cdot}H_2O$	IV + III
Hollandite #1	Sorharas, Lappland, Sweden	$(Mn^{(IV)},Al,Si)_{6.8}(Fe,Mn^{(III)})_{1.1}\ (Ba,K,Pb,Na)_{1.0}O_{16}$	IV + III
Hollandite #2[a]	Yavapai, AZ, USA	$Ba_{0.8}Pb_{0.1}K_{0.3}Cl_{0.3}S_{0.1}Ti_{0.4}\ Mn_{7.1}Fe_1Si_{1.1}Al_{1.1}O_{16}$	IV + III
Hollandite #3	Kajlidongri, Madhya Pradesh, India	$Ba_{0.8}Pb_{0.2}Na_{0.1}Mn^{(IV)}_{6.1}\ Fe^{(III)}_{1.3}Mn^{(III)}_{0.5}Al_{0.2}Si_{0.1}O_{16}$	IV + III
Cryptomelane	Reaphook Hill, Blinman, SA, Australia	$(K_{0.9},Ba_{0.1})Mn_8O_{16}$	IV
Coronadite	Broken Hill, NSW, Australia	$Pb_{1.1}Ba_{0.1}Mn^{(IV)}_{7.2}Mn^{(III)}_{0.5}\ V^{(V)}_{0.2}Al_{0.1}O_{16}$	IV + III
Chalcophanite #1	"Glory Hole", Gold Hill mine, Tooele, UT, USA	$(Zn,Fe,Mn)Mn_3O_7{\cdot}3H_2O$	IV + III
Chalcophanite #2	Mapimi, Durango, Mexico	$(Zn,Fe,Mn)Mn_3O_7{\cdot}3H_2O$	IV + III
Hydrohetaerolite	"Glory Hole", Gold Hill mine, Tooele, UT, USA	$Zn_2Mn^{(III)}_4O_8{\cdot}H_2O$	III
Lithiophorite #1	Mt Hamilton, Santa Clara Co, California, USA	$LiAl_2(Mn^{(III)}Mn^{(IV)}_2)O_6(OH)_6$	IV + III
Lithiophorite #2	Postmasburg, Northern Cape, RSA	$LiAl_2(Mn^{(III)}Mn^{(IV)}_2)O_6(OH)_6$	IV + III

Samples are from the author's collection except:

[a] Stanford University mineral collection

[b] in fact, a hausmannite (to which braunite is often confused in the specimens from that location)

[c] Ecole Nationale Supérieure des Mines de Paris

suggested also by XRD); this is often confused in the samples from that locality. But the manganese XANES data indicate that hausmannite is more abundant than braunite in the sample, which was difficult to evaluate based on XRD methods alone. Similarly, the franklinite from New Jersey (MnO ~6.3(2) wt. %) shows pre-edge information typical of dominantly Mn(II) in a site of T_d geometry, in agreement with its compositional stoichiometry information.

More complex oxides: braunite, aurorite, rancieite

In contrast to hausmannite, the average valence of manganese in the "braunite #2", aurorite, and rancieite samples is found to be close to 4 (Table 3), suggesting the absence of detectable amounts of reduced states of manganese (±10 mol%; see below). However, the compositional stoichiometric analysis of the total oxygen and manganese obtained by electron microprobe analyses of rancieite suggests a model fraction of Mn(II) of 7 wt. %, which is close to our estimate from the pre-edge region. In a second braunite sample (from India), which was verified by XRD to be braunite, as well as in aurorite, the amount of Mn(II) predicted from compositional stoichiometry is ~10 atom %. However, in these samples, the pre-edge information does not provide conclusive evidence for the presence of Mn(II) inferred from compositional stoichiometry (provided that this last method is actually that reliable). This result confirms that the sensitivity of the manganese pre-edge method presented here is 10 atom %. This level of sensitivity makes XANES useful for the measurement of average valences of manganese.

The case of n'sutite

N'sutite ("δ-MnO_2") has been shown to be a complex mixture of highly defective domains of pyrolusite and ramsdellite with tunnel structures that can contain hydroxyls and a variety of charge compensating cations, which should stabilize some Mn(III) (Turner and Buseck 1979, 1983). The amount of Mn(III) in that n'sutite sample can be estimated from linear combinations of pre-edge data for end-members (Mn(III) and Mn(IV) are centered at 6540.9 and 6541.5 eV, respectively). The calculated fraction of trivalent manganese (0.30(5)) is much higher than that estimated from considerations of stoichiometry (based on electron microprobe analyses, which suggests 0.20(5) mole fraction of Mn(III)). Estimation of the average

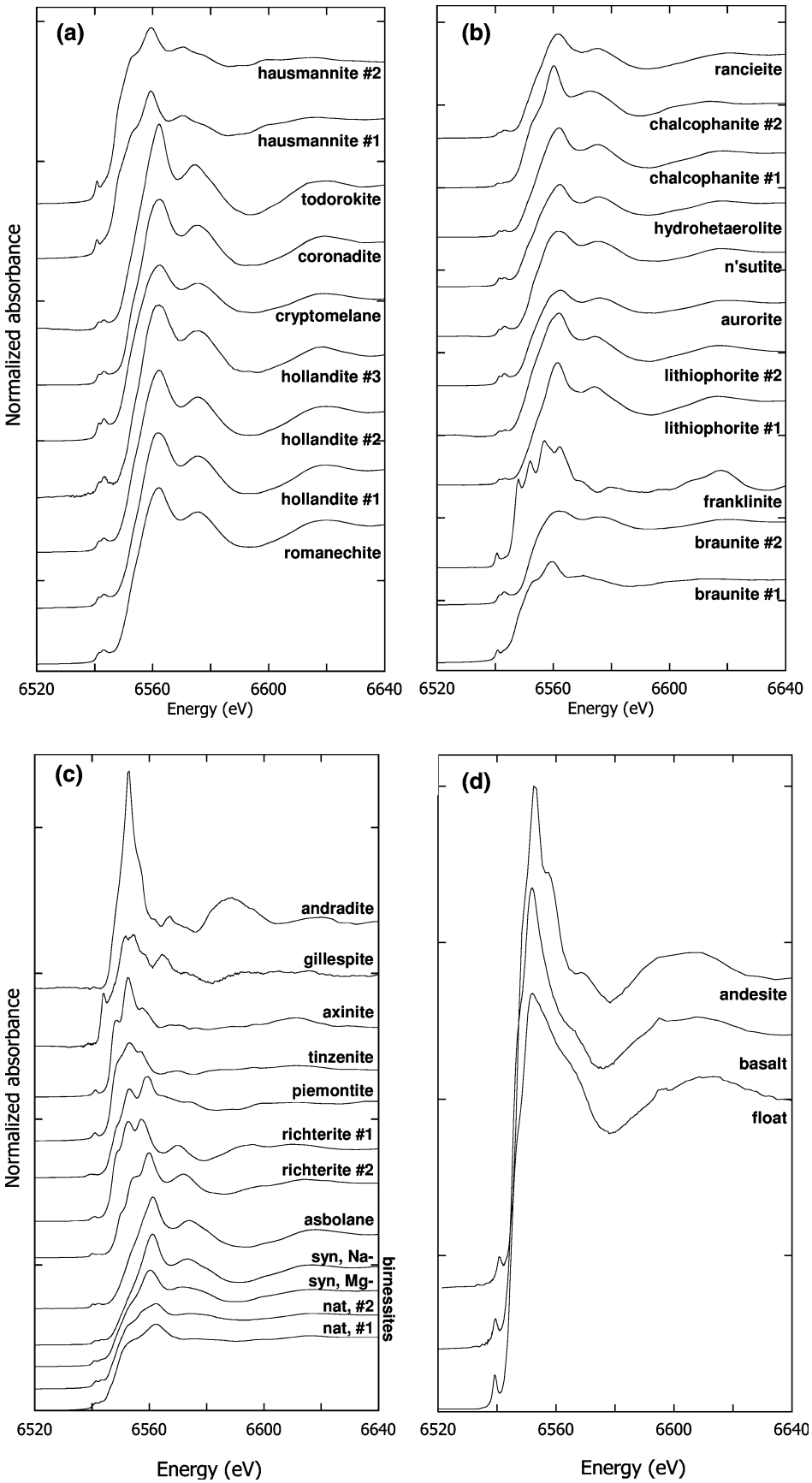

Fig. 2 Selected Mn K-edge XANES spectra for the "test" samples (**a**, **b**) and for the "unknown" samples (**c**, **d**), used to evaluate their manganese valence and their symmetry environment (Tables 2, 3, 4, 5 list their respective mineralogical and pre-edge information)

Table 3 Pre-edge information for the "test" samples and their valence and local Mn-symmetry environment evaluation

Sample	Pre-edge energy (eV)	Pre-edge area	Centroid (eV)	Integrated area	Estimated average valence	Estimated symmetry environment
Hausmannite #1	6540.02	0.0131	6540.89	0.1740	2.6	$T_d + O_h$
	6540.69	0.1309				
	6542.11	0.0299				
Hausmannite #2	6539.57	0.0097	6540.87	0.2204	2.6	$T_d + O_h$
	6540.70	0.1755				
	6542.10	0.0352				
Braunite #1	6540.12	0.0237	6540.89	0.1956	2.6	$T_d + O_h$
	6540.68	0.1342				
	6542.14	0.0377				
Braunite #2	6541.10	0.0489	6541.65	0.1300	4.2	O_h
	6541.55	0.0470				
	6542.59	0.0341				
Franklinite	6540.45	0.2301	6540.57	0.2552	2.0	$T_d + O_h$
	6541.71	0.0251				
Aurorite	6540.67	0.0097	6541.60	0.1426	4.1	O_h
	6541.38	0.1023				
	6541.60	0.0306				
Rancieite	6540.73	0.0152	6541.61	0.0697	4.1	O_h
	6541.40	0.0345				
	6542.64	0.0200				
N'sutite	6540.39	0.0171	6541.32	0.1290	3.5	O_h
	6541.27	0.0900				
	6542.26	0.0218				
Romanechite	6540.43	0.0081	6541.29	0.0775	3.4	O_h
	6541.20	0.0550				
	6542.11	0.0143				
Rodorokite	6540.64	0.0069	6541.44	0.0791	3.9	O_h
	6541.33	0.0565				
	6542.18	0.0157				
Hollandite #1	6540.59	0.0114	6541.42	0.0825	3.7	O_h
	6541.30	0.0531				
	6542.27	0.0183				
Hollandite #2	6540.71	0.0102	6541.42	0.0790	3.7	O_h
	6541.24	0.0527				
	6542.45	0.0161				
Hollandite #3	6540.24	0.0035	6541.44	0.0792	3.7	O_h
	6541.36	0.0681				
	6542.77	0.0076				
Cryptomelane	6540.59	0.0135	6541.55	0.1614	4.0	O_h
	6541.36	0.1129				
	6542.52	0.0350				
Coronadite	6540.49	0.0082	6541.43	0.0917	3.7	O_h
	6541.34	0.0715				
	6542.60	0.0120				
Chalcophanite #1	6540.37	0.0096	6541.37	0.0934	3.6	O_h
	6541.36	0.0742				
	6542.43	0.0096				

Table 3 continued

Sample	Pre-edge energy (eV)	Pre-edge area	Centroid (eV)	Integrated area	Estimated average valence	Estimated symmetry environment
Chalcophanite #2	6540.47	0.0142	6541.49	0.1517	3.8	O_h
	6541.37	0.1096				
	6542.45	0.0279				
Hydrohetaerolite	6540.26	0.0160	6541.04	0.0777	2.9	O_h
	6540.97	0.0395				
	6541.74	0.0222				
Lithiophorite #1	6540.52	0.0048	6541.35	0.0660	3.6	O_h
	6541.33	0.0522				
	6542.91	0.0091				
Lithiophorite #2	6540.61	0.0092	6541.37	0.0876	3.6	O_h
	6541.29	0.0572				
	6541.91	0.0212				

valence of manganese using the XANES pre-edge method presented here should be more accurate than an estimate based on stoichiometry, which relies on an accurate measurement of the total oxygen content of the mineral (including hydroxyls). Finally, the Mn K-edge XANES of n'sutite (Fig. 2b) shows broad features (as in ramsdellite or more complex oxyhydroxides such as hollandite or chalcophanite). This suggests that the pyrolusite-type domains (which promote highly structured XANES signatures) do not predominate in the n'sutite sample examined in this study (<1/4 in volume, i.e., less than the aperiodic, defective domains containing either Mn(III) or Mn(IV)).

The mixed oxides romanechite (psilomelane) and todorokite

The studied romanechite (Fig. 2a and Tables 2, 3) shows an average valence of manganese of 3.4(5), which is consistent with its structural formula ($\sim Ba_{0.7}Mn(III)_{1.3}Mn(IV)_{3.7}O_{10}\cdot 1–1.5(H_2O)$) in which a significant proportion of Mn(III) is required to charge balance the "tunnel-ions", such as barium (Turner and Post 1988). In the studied todorokite sample, however, the pre-edge centroid is close to Mn(IV) (3.9), suggesting that few substitution of Mn(III) occurred within the four sites for manganese in that structure (Post and Bish 1988). This slight evidence of Mn(III) (<10%) is in agreement with Post et al. (2003).

The complex oxides of the hollandite family: hollandite, cryptomelane, and coronadite

In hollandite (Post et al. 1982; Kudo et al. 1990), tunnels formed by $Mn(IV)O_6^{8-}$ octahedral contain mono-, and divalent charge-compensating cations. As for other manganohydroxides, the cations are balanced also by a variety of cations, such as Al^{3+}, Si^{4+}, Fe^{3+}, and Mn^{3+}. Three hollandites of similar compositions (see Fig. 2a and Tables 2, 3) yielded pre-edge information consistent with the presence of dominant amounts of Mn(IV), which is octahedrally coordinated, based on their high-energy XANES regions. Detectable amounts of Mn(III) or Mn(II) are found in the sample from the type locality in India (centroid at 6541.44 eV). Assuming that the calculated structural formula for that sample ($\sim (Ba,Pb,Na)_{1.1}Mn(IV)_{6.1}(Fe,Mn(III))_{0.8}(Al,Si)_{0.3}O_{16}$), 8.0(5) atom % Mn(III) is predicted in that sample. Similarly, the two other samples ("hollandite #1" and "hollandite #2" from Lappland and Arizona, respectively) also show ~85(5) atom % Mn(IV). Despite the fact that the pre-edge is not sensitive to these relatively low concentrations, the other manganese cations must be trivalent, as for romanechite. For the hollandite from Lappland (Sweden, $\sim (Ba,K,Pb,Na)_{1.0}Mn(IV)_{6.3}(Fe,Mn(III))_{1.1}(Al,Si)_{0.5}O_{16}$), the calculated amount of Mn(III) is 16(5) atom %, which is in good agreement with the pre-edge information. The cryptomelane sample from Australia could be used as another model for Mn(IV), as no detectable amount of reduced manganese species can be detected (<10 atom %). In contrast, the lead end-member coronadite ($\sim Pb_{1.1}Ba_{0.1}Mn(IV)_{7.2}Mn(III)_{0.5}V(V)_{0.2}Al_{0.1}O_{16}$) has a pre-edge very similar to that for the other hollandites (*sensu-stricto*) of the present study i.e., with an average manganese valence of 3.7(5). This result is slightly higher than that obtained from stoichiometry considerations based on electron microprobe analysis (93(2) atom % of Mn(IV) is equivalent to an average valence for manganese of 3.9(1)).

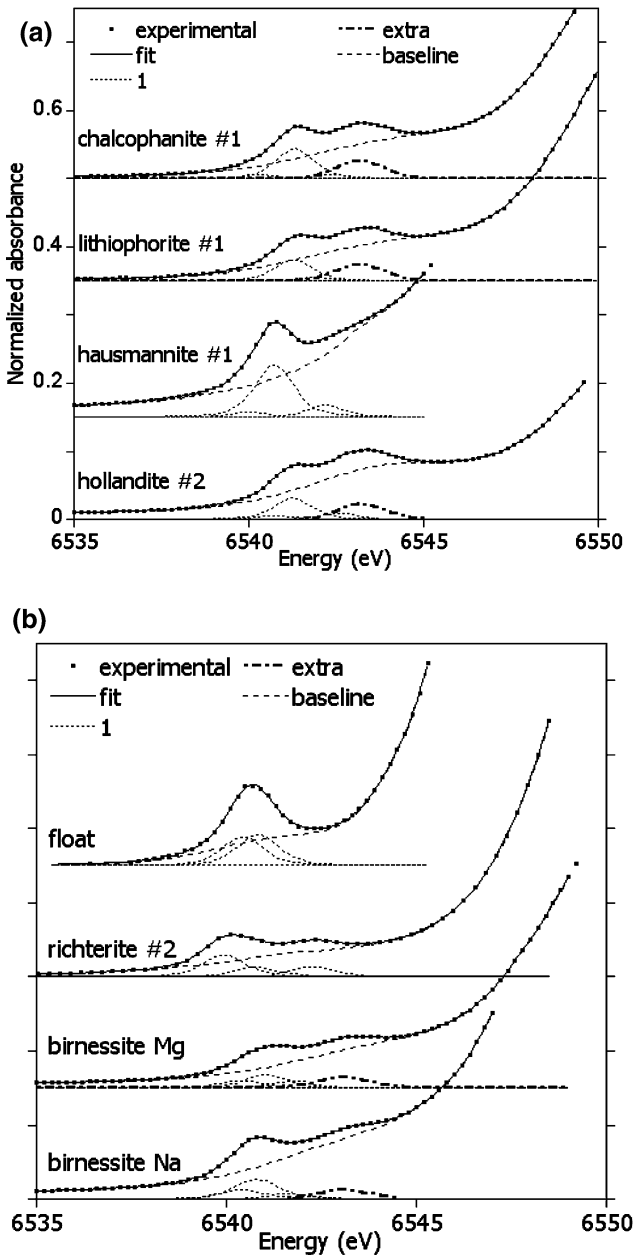

Fig. 3 Selected of pre-edge deconvolutions for a selection of "test" samples (**a**) and of "unknown" samples (**b**), used to evaluate their manganese valence and their symmetry environment

Phyllomanganates: chalcophanite, hydrohetaerolite, and lithiophorite

In these phyllomanganates, one of the seven sites for manganese is vacant within the $Mn(IV)O_6$ layers (Post and Appleman 1994). Pre-edge information for the chalcophanite sample from Mexico (chalcophanite #2) is consistent with octahedrally Mn(IV), in good agreement with its crystal structure. Pre-edge information for the chalcophanite sample from Utah ("chalcophanite #1) is consistent with dominant amounts of Mn(IV) in O_h symmetry, in agreement with its ideal formula ($ZnMn_3O_7{\cdot}3H_2O$). Because the geometry is identical among the two sites in chalcophanite (O_h), the pre-edge feature varies linearly with Mn valence (Wilke et al. 2001). Consequently, we can extract the atomic fraction of Mn(III) in that model: ~10(3) atom % Mn, probably arising from tiny inclusions of hydrohetaerolite ($Zn_2Mn(III)_4O_8{\cdot}H_2O$), with which chalcophanite is often associated in the samples from the Glory mine (UT, USA).

A sample of hydrohetaerolite from that locality, which could finally be separated using optical microscopy methods, confirms the presence of dominant amounts of Mn(III), based on a pre-edge centroid at the predicted value for trivalent manganese (6541.04 eV).

Finally, two lithiophorites were studied, including well-developed single crystals from Postmasburg, South Africa ("lithiophorite #2"). The two studied samples show very consistent manganese valence information (average manganese valence of 3.6). This result is in excellent agreement with their structural formula ($LiAl_2(Mn(III)Mn(IV)_2)O_6(OH)_6$), suggesting that 1/3 of the manganese should be trivalent to charge-compensate for the coupled (Al–Li) substitution.

Application to "unknowns": complex oxides and silicates of geochemical interest

Figure 2c, d and Tables 4, 5 show the Mn K-edge and pre-edge information derived for a collection of minerals (and three glasses, incl. two natural ones) of geochemical interest for which no information on the actual valence of manganese was previously available. Figure 3b shows some models performed on the pre-edge region for selected "unknown" samples.

Rock-forming silicates: richterite, axinite, garnet, piemontite

Two richterites ("richterite #1" and "richterite#2"), two axinite-related minerals (ferromanganoaxinite and tinzenite), one andradite garnet and one piemontite were studied. In the piemontite from the St Pierre and Miquelon French archipelago (North America), the measured average valence of manganese is 3.2(2). In this mineral, manganese substitutes for Al and Fe in the octahedral sites (Bonazzi et al. 1992). Consequently, the measured valence of 3.2 is consistent with the presence of dominant amounts of Mn(III) in octahedral sites of that sorosilicate, in excellent agreement with its crystal chemistry. Straightforward conclusions can also be drawn for the Mn-bearing andradite (MnO ~0.21(6) wt. %), which Mn K-edge XANES is similar to that for spessartite ($Mn_3Al_2Si_3O_{12}$), in which divalent manganese occupies the A site, of dodecahedral symmetry (Novak

Table 4 Mineralogical information for the "unknown" samples

Sample	Origin	Formula	Supposed valence
Piemontite[a]	St Pierre et Miquelon Isl., North America, France	$(Mn,Ca)LaAlMn_2[SiO_4][Si_2O_7]O(OH)$	II
Mn-andradite[a]	Unknown locality, Mexico	$(Ca_{2.5}Fe_{0.4}Mn_{0.01})(Fe_{1.1}\ Al_{0.2}Ti_{0.8})Si_3O_{12}$	II
Richterite #1[b]	Synthetic	$(K,Na)(Na,Ca)(Mg,Mn,Fe)_5Si_8O_{22}(OH,F)_2$	II + III
Richterite #2[b]	Synthetic	$(K,Na)(Na,Ca)(Mg,Mn,Fe)_5Si_8O_{22}(OH,F)_2$	II (+III)
Tinzenite	Molinello, Genoa, Italy	$Ca_{1.9}Mn_{0.8}Fe^{2+}{}_{0.3}Al_2(BO_3)Si_4O_{12}(OH)$	II + III
Axinite[a]	La Gardette, Isère, France	$Ca_{3.9}(Mn_{0.6},Fe^{(II)}{}_{0.7},Mg_{0.4})(Al_4,\ Fe^{(III)}_{0.1})\ (BO_3)_2\ OH_{1.9}(SiO_3)_4$	III
Gillespite	Tres Pozos, Baja California, Mexico	$Ba(Fe_{0.98},Mn_{0.02})Si_2O_8$	II
"Birnessite" #1[c]	Mont Saint Hilaire, QC, Canada	$\sim(Na,Ca,K)(Mg,Mn)Mn_6O_{14}{\cdot}5H_2O$	IV + III
"Birnessite" #2[c]	Mont Saint Hilaire, QC, Canada	$\sim(Na,Ca,K)(Mg,Mn)Mn_6O_{14}{\cdot}5H_2O$	IV + III
Birnessite-Mg	synthetic	$MgMn_6O_{14},{\cdot}xH_2O$	IV + III
Birnessite-Na	synthetic	$NaMn_6O_{14},{\cdot}xH_2O$	IV + III
Absolane	Near Porterville, Tulare County, CA, USA	Unknown mixture of various oxi-hydroxides	IV + III
Float glass	synthetic (1,450°C/5 h)	$\sim Na_{0.99}Ca_{0.92}Mg_{0.04}Al_{0.15}Si_{3.16}O_8$ (+ 0.3 wt.% Mn) NBO/T = 0.8	II
Basaltic glass[d]	−4,500 m, Mid Ocean Ridge, North Atlantic "92 DS" drilling	MORB composition with a NBO/T (non-bridging oxygen per tetrahedron ratio) of 0.82	II
Andesite glass[d]	−4,500 m, Mid Ocean Ridge, North Atlantic "SRI DR04 (19769)" drilling	MORB composition with a NBO/T (non-bridging oxygen per tetrahedron ratio) of 0.62	II

Samples are from the author's collection except:

[a] sample from the Ecole Nationale Supérieure des Mines de Paris

[b] sample kindly from the Ph.D. work of Arnaud Papin and Jean-Louis Robert, CNRS, Orléans, France

[c] samples from the Canadian Museum of Nature/Musée Canadien de la Nature, Ottawa (kindly provided by P. Piilonen), from a pseudomorphosis of rhodocrosite

[d] sample kindly from the Ph.D. work of Antoine Bézos, IPG Paris, France

and Gibbs 1971). Hence, the very low pre-edge feature for that andradite, centered very close to the centroid for divalent manganese and a medium-range environment typical of a garnet structure.

The two richterites show variable manganese valences. The sample "richterite #1" is the most oxidized, with an average manganese valence state of 2.5(2), whereas "richterite #2" is more reduced (average manganese valence of 2.1(2)). In these amphiboles, there are three octahedral sites (M1, M2, M3) and one antiprism pseudo-cubic M4 site available for manganese (Oberti et al. 1993). Also, the presence of higher valences (such as Mn(III)) is reported, as a result of charge-compensation with network modifiers (such as alkali and alkali-earth elements). Based on these spectra, electron microprobe analysis, and infrared spectroscopy, Papin (2001) found that the valence of manganese is correlated with the local, or total, absence of protons in the structure, such as in ungarettiite $(NaNa_2(Mn(II)_2Mn(III)_3)Si_8O_{22}O_2)$.

Finally, in the two studied axinite-type cyclosilicates, the average manganese valence is lower [2.7 and 3.0(5) for tinzenite (intermediate member between the Mn-rich and the Fe-rich poles) and ferroaxinite, respectively]. This result is unexpected as manganese is thought to be only divalent in such minerals (see Andreozzi et al. 2000). However, Mossbauer spectroscopy has shown that ferrous and ferric iron coexists in such minerals (e.g., up to 25 atom % in the samples from the Bourg d'Oisans in the French Alps; see Andreozzi et al. 2000). Therefore, trivalent manganese is also possible, as the MnO/Mn_2O_3 buffer exists at much higher oxygen fugacities than the quartz-fayalite-magnetite buffer. Our XANES measurements indicate that variations in the valence of manganese should be taken into account (as for iron) to derive more accurate structural formula for axinites.

Table 5 Pre-edge information for the "unknown" samples and their valence and local Mn-symmetry environment evaluation

Name	Pre-edge energy (eV)	Pre-edge area	Centroid (eV)	Integrated area	Estimated average valence	Estimated symmetry environment
Piemontite	6540.00	0.0267	6540.97	0.0819	3.2	O_h
	6540.98	0.0334				
	6542.14	0.0218				
Mn-andradite	6540.24	0.0161	6540.67	0.0497	2.0	[8]
	6540.88	0.0335				
Richterite #1	6540.04	0.0382	6540.83	0.1035	2.5	O_h
	6540.99	0.0505				
	6542.36	0.0149				
Richterite #2	6539.93	0.0514	6540.67	0.0971	2.1	O_h
	6540.76	0.0226				
	6542.19	0.0232				
Tinzenite	6539.92	0.0137	6540.85	0.1435	2.7	O_h
	6540.70	0.0740				
	6541.27	0.0558				
Axinite	6540.10	0.0218	6540.91	0.1246	3.0	O_h
	6541.06	0.1004				
	6542.21	0.0024				
Gillespite	6540.15	0.0595	6540.66	0.0870	2.0	C_4
	6541.77	0.0274				
Birnessite #1	6540.46	0.0225	6541.14	0.1003	3.1	O_h
	6541.29	0.0753				
	6542.75	0.0025				
Birnessite #2	6540.40	0.0209	6541.13	0.1092	3.1	O_h
	6541.18	0.0577				
	6541.53	0.0306				
Birnessite-Mg	6540.42	0.0159	6541.03	0.0620	2.9	O_h
	6541.00	0.0296				
	6541.67	0.0165				
Birnessite-Na	6540.35	0.0215	6540.75	0.0799	2.3	O_h
	6540.73	0.0462				
	6541.52	0.0122				
Absolane	6540.39	0.0050	6541.28	0.0702	3.4	O_h
	6541.35	0.0652				
Float	6540.44	0.0658	6540.63	0.1372	2.0	(glassy)
	6540.82	0.0714				
Basaltic glass	6540.46	0.0531	6540.77	0.1128	2.5	(glassy)
	6541.04	0.0596				
Andesite glass	6540.09	0.0286	6540.58	0.1008	1.8	(glassy)
	6540.77	0.0722				

Gillespite

In the gillespite sample examined, the manganese pre-edge was too low in intensity and noisy to be accurately observed because of the low manganese concentration (MnO $\sim$0.13(8) wt. %) and interferences from the Ba L-edges. However, given the position of the edge and the first EXAFS oscillation, manganese is divalent and is located in a centrosymmetric site with very short Mn–O distances, which is incompatible with octahedral symmetry environment. Also, another pre-edge feature is observed near 6545 eV (see Fig. 2c), which has not been observed in any other compound of the present study. In fact, the Mn K-edge XANES spectrum for gillespite is very close to that

measured at the Fe K-edge for the same sample (Wilke et al. 2001). Iron in gillespite is coordinated by four oxygens in square planar geometry (Pabst 1943). Such an intense pre-edge feature is related to electronic transitions from 1s to 4d levels, which are allowed for centrosymmetric sites. We conclude from these observations that manganese is dominantly divalent and substitutes for divalent iron in gillespite.

Synthetic and natural birnessites

Mn K-edges XANES spectra were collected for a series of four birnessites (layered phyllomanganates such as lithiophorites). Among these birnessites, two samples are natural pseudomorphs after rhodocrosite from Mont St Hilaire, Québec and have not been described before (their tentative identification as "birnessite" is related to their Mn-rich chemical composition and poor crystallinity). For comparison, two synthetic birnessites were also studied (which are considered as analogues to the natural ones: see Lanson et al. 2002). In this study, we will focus only on the valence of manganese in these phases, as the structures of these minerals have been the subject of many recent papers (see, e.g., Lanson et al. 2002; Gaillot et al. 2003, 2007). In synthetic birnessites, manganese is expected to be predominantly tetravalent with some Mn(III) to charge balance various cations and trace amounts of Mn(II). Must of these substituted Mn(III) are bound above the vacant sites present in the Mn O_h layer (Manceau et al. 2002). The measured average manganese valence of the two synthetic birnessites is between 2.3 and 2.9 ($\sim$3.7 for a monoclinic/triclinic Na-birnessite; Post and Veblen 1990; Lanson et al. 2002; as up to 1/3 of the manganese in these phases is trivalent; Drits et al. 1997). Moreover, the position of the main edge for the Na-birnessite is coherent with the low valence extracted from the pre-edge. Therefore, the disagreement is large between the pre-edge valence and the chemistry information on these compounds and could be due to an artifact of sample preparation. So further studies are required to fully determine the valence of manganese in these birnessites and the potential effect of beam photoreduction (despite we did not observed any). We note, however, that the two natural "birnessites" from Mont St Hilaire ($\sim$(Na,Ca,K)(Mg,Mn)$Mn_6O_{14}\cdot 5H_2O$) show a comparable manganese valence (3.1) coherent with the synthetic Mg-birnessite. A possible explanation would be that these birnessites may contain variable amounts of reduced manganese under a cryptocrystalline form that remains to be identified, such as a manganese equivalent for fougerite (or "green rust" (Fe(II), $Mg)_6Fe(III)_2(OH)_{18}\cdot 4H_2O$; Abdelmoula et al. 1998) of composition involving Mn(II), Mn(III) and hydroxyls, despite the fact that this kind of layered double hydroxides has never been encountered before by TEM analyses.

Absolane

Finally, a typical nickel-rich manganese ore that miners called "absolane" was studied. This "absolane" shows an average manganese valence of manganese of 3.4(5), which is close to the valence of manganese in lithiophorites investigated in this study, in agreement with Post (1999). In fact, the Mn K-edge XANES spectrum for the absolane sample from California shows similarities to the manganese XANES spectra of lithiophorites. However, they are markedly different from the XANES results of psilomelane and many other Mn(IV)-bearing oxyhydroxides investigated here. Because the Mn K-edge XANES probes a fairly large volume around the central absorbing manganese (radial distance of 5–10 Å), our spectroscopic information supports the idea that the crystal structure of lithiophorite is a good model for the structural networks in absolane, which contains more transition elements than lithiophorite (see Chukhrov et al. 1980a, b; Manceau et al. 1987).

Manganese in silicate glasses (MORB and float)

Recently, Bézos and Humler (2005) tried to determine the oxygen fugacities for various mid-ocean ridge basalts (MORB), based on the Fe(II)/Fe(III) ratios measured either by wet chemistry methods or electron microprobe analyses (Fialin et al. 2004). Although iron is the main valence-sensitive cation in magmas, manganese is also sensitive to oxygen fugacity conditions, particularly under oxidizing conditions. Our Mn K-edge XANES measurement on two natural glasses (a glassy tholeitic basalt and an andesite) from the mid-Atlantic ridge confirms that manganese is dominantly divalent in that glass (average valence is 2.5 and 1.8(5), respectively). These values are representative of the quenched magma at its glass transition temperature. The pre-edge intensity is relatively high for Mn(II) in a centrosymmetric site such as square planar, octahedral or cubic. However, similar pre-edge features were also observed for divalent iron and nickel in many other glass/melts compositions (see Farges et al. 2001; Jackson et al. 2005). The combination of a variety of different spectroscopic and ab initio methods has proven that a continuum of environments (from T_d to O_h) exists in silicate glasses and melts around Fe(II) and Ni(II). This distribution of site is centered on a type of trigonal bipyramid (5-coordinated). Like around Fe(II) and Ni(II), the pre-edge information at the Mn K-edge in the silicate glasses studied here suggests the presence of a mixture of symmetry environments similar to these observed around Fe(II) and Ni(II). However, the pre-edge feature integrated area is higher for the float glass and lower for the andesite (intermediate for the basalt). This suggests that the glass composition (particularly the amount and type of network modifiers) has a large

influence on the average manganese speciation. As for Fe(II) and Ni(II), the glass network appears richer in manganese located in non-centrosymmetric environments (likely tetrahedral and trigonal bipyramids) with increasing alkali contents.

Conclusion

Analysis of the pre-edge spectra of manganese in model compounds and mixtures shows that it is possible to derive average manganese valence information from the centroid of the pre-edge position, with 5% accuracy on average. The pre-edge intensities for manganese follow trends similar to those already described for other transition elements (e.g., titanium, iron, nickel etc.), as a function of site distortion.

The application of the XANES pre-edge method presented here to "test" minerals provides estimates of manganese valence that are generally consistent with those from other methods. Application of this method to "unknown" samples of geochemical interest (such as rock-forming minerals, glasses, soils-based oxyhydroxides) provides consistent information on manganese valence (e.g., piemontite, hollandite) and new information (e.g., as in axinites). In poorly crystalline oxyhydroxides, more reduced valence of manganese is detected, but this result needs to be crosschecked by other methods. This method provides structural information for various types of Earth materials in which manganese plays a major role. The method is also applicable to micro-XANES measurements on small and diluted samples as precious minerals or patrimonial materials (Chalmin et al. 2006; Reiche and Chalmin 2008).

Acknowledgments We gratefully acknowledge Arnaud Papin (formerly at CNRS, Orléans), Ina Reiche (Laboratoire de Recherche des Musées de France, UMR171 CNRS, Paris), and Antoine Bézos (IPGP, Paris) for providing some of the samples from their Ph.D. work. We also thank the mineral collections of the Ecole des Mines de Paris (J.M. Le Cleac'h and A. Djemai), the Centre Canadien de la Nature in Ottawa (P. Piilonen), the Laboratoire de Minéralogie-Cristallographie de Paris ("Sorbonne collection"; J.C. Bouillard), and Stanford University for providing some of the specimens used in this study (the others are from the private collection of François Farges). The staffs of SSRL (especially Joe Rodgers, Cathy Knotts, and Michelle Steger) and ESRF (especially Jean Susini on ID21) are thanked for their help. Helpful discussions with John R. Rehr (University of Washington at Seattle, USA) on FEFF calculations and P. Glatzel (ESRF, Grenoble, France) on multiplet calculations are also acknowledged.

References

Abdelmoula M, Trolard F, Bourrié G, Génin J-MR (1998) Evidence for the Fe(II)-Fe(III) green rust "Fougerite" mineral occurrence in a hydromorphic soil and its transformation with depth. Hyperfine Interact 112:235–238. doi:10.1023/A:1010802508927

Andreozzi GB, Ottolini L, Lucchesi S, Graziani G, Russo U (2000) Crystal chemistry of the axinite-group minerals: a multi-analytical approach. Am Mineral 85:698–706

Bargar JR, Tebo BM, Villinski JE (2000) In situ characterization of Mn(II) oxidation by spores of the marine *Bacillus* sp. strain SG–1. Geochim Cosmochim Acta 64(16):2775–2778. doi:10.1016/S0016-7037(00)00368-9

Baron V, Gutzmer J, Rundlof H, Tellgren R (1998) The influence of iron substitution on the magnetic properties of hausmannite, Mn(Fe, Mn)2O4. Am Mineral 83:786–793

Belli M, Scafati A, Bianconi A, Mobilio S, Palladino L, Reale A et al (1980) X-ray absorption near edge structures (XANES) in simple and complex Mn compounds. Solid State Commun 35:355–361. doi:10.1016/0038-1098(80)90515-3

Bézos A, Humler E (2005) The $Fe^{3+}/\Sigma Fe$ ratios of MORB glasses and their implications for mantle melting. Geochim Cosmochim Acta 69(3):711–725

Bonazzi P, Garbarino C, Menchetti S (1992) Crystal chemistry of piemontites: REE-bearing piemontite from Monte Brugiana, Alpi Apuane, Italy. Eur J Mineral 4:23–33

Burns RG (1993) Mineralogical applications of crystal field theory, 2nd edn. Cambridge University Press, Cambridge, 551 p

Calas G (1984) Electron paramagnetic resonance. Rev Mineral 18:513–571

Chalmin E, Vignaud C, Salomon H, Farges F, Susini J, Menu M (2006) Minerals discovered in paleolithic black pigments by transmission electron microscopy and micro-X-ray absorption near-edge structure. Appl Phys A 83(2):213–218. doi:10.1007/s00339-006-3510-7

Chukhrov FV, Gorshkov AI, Vitovskaya IV, Drits VA, Sivtsov AI, Dikov YP (1980a) Crystallochemical nature of Co–Ni asbolane. Izv Akad Nauk SSSR Ser Geol 6:73–81

Chukhrov FV, Gorshkov AI, Vitovskaya IV, Drits VA, Sivtsov AV (1980b) Crystallochemical nature of Ni-asbolane. Izv Akad Nauk SSSR Ser Geol 9:108–120

Dräger G, Frahm R, Materlik G, Brummer O (1988) On the multipole character of the X-ray transitions in the pre-edge structure of Fe K absorption spectra. Phys Status Solid B 146:287–293. doi:10.1002/pssb.2221460130

Dräger G, Kirchner T, Bocharov S, Kao CC (2001) Spin-resolved NEXAFS from resonant X-ray scattering (RXS). J Synchrotron Radiat 8:398–400. doi:10.1107/S0909049500017234

Drits VA, Silvester EJ, Gorshkov AI, Manceau A (1997) The structure of monoclinic Na-rich birnessite and hexagonal birnessite. Part 1. Results from X ray diffraction and selected area electron diffraction. Am Mineral 82:946–961

Drits VA, Lanson B, Bougerol-Chaillout C, Gorshkov AI, Manceau A (2002) Structure of heavy-metal sorbed birnessite: part 2. Results from electron diffraction. Am Mineral 87:1646–1661

Farges F (2005) *Ab initio* and experimental pre-edge investigations of the Mn K-edge XANES in oxide-type materials. Phys Rev B 71:155109. doi:10.1103/PhysRevB.71.155109

Farges F (2008) Chromium speciation in oxide-type compounds. Application to minerals, gems, aqueous solutions and silicate glasses. Phys Chem Miner (in press)

Farges F, Brown GE Jr, Rehr JJ (1996) Coordination chemistry of Ti(IV) in silicate glasses and melts: I. XAFS study of titanium coordination in oxide model compounds. Geochim Cosmochim Acta 60:3023–3038. doi:10.1016/0016-7037(96)00144-5

Farges F, Brown GE Jr, Rehr JJ (1997) Ti K-edge XANES studies of Ti-coordination and disorder in oxide compounds: comparison between theory and experiment. Phys Rev B 56:1809–1819. doi:10.1103/PhysRevB.56.1809

Farges F, Brown GE Jr, Petit PE, Munoz M (2001) Transition elements in water-bearing silicate glasses/melts. Part I. A high-resolution and anharmonic analysis of Ni coordination environments in crystals, glasses, and melts. Geochim Cosmochim Acta 65(10):1665–1678

Farges F, Lefrère Y, Rossano S, Berthereau A, Calas G, Brown GE Jr (2004) The effect of redox state on the local structural environment of iron in silicate glasses: a combined XAFS spectroscopy, molecular dynamics, and bond valence study. J Non Cryst Solids 344(3):176–188. doi:10.1016/j.jnoncrysol.2004.07.050

Farges F, Chalmin E, Vignaud C, Pallot-Frossard I, Susini J, Bargar J et al (2005) Archeological applications of XAFS: prehistorical paintings and medieval glasses. Phys Scr T115:885–887. doi:10.1088/0031-8949/2005/T115/264

Fialin M, Bézos A, Wagner C, Magnien V, Humler E (2004) Quantitative electron microprobe analysis of Fe3+/∑Fe: basic concepts and experimental protocol for glasses. Am Mineral 89:654–662

Gaillot AC, Flot D, Drits VA, Manceau A, Burghammer M, Lanson B (2003) Structure of synthetic K-rich birnessite obtained by high-temperature decomposition of $KMnO_4$. Chem Mater 15:4666–4678. doi:10.1021/cm021733g

Gaillot AC, Drits VA, Manceau A, Lanson B (2007) Structure of synthetic K-rich phyllomanganate birnessite obtained by high-temperature decomposition of $KMnO_4$ substructures of K-rich birnessite from 1000°C experiment. Microporous Mesoporous Mater 98(1–3):267–282. doi:10.1016/j.micromeso.2006.09.010

Garvie LAJ, Craven AJ, Brydson R (1994) Use of electron-energy loss near-edge fine structure in the study of minerals. Am Mineral 79:411–425

Gilbert B, Frazer BH, Belz A, Conrad PG, Nealson KH, Haskel D et al (2003) Multiple scattering calculations of the bonding and X-ray absorption spectroscopy of manganese oxides. J Phys Chem 107:2839–2847

Glatzel P, Bergmann U (2005) High resolution 1 s core hole X-ray spectroscopy in 3d transition metals complexes—electronic and structural information. Coord Chem Rev 249:65–95. doi:10.1016/j.ccr.2004.04.011

Glatzel P, Bergmann U, Yano J, Visser H, Robblee JH, Gu W et al (2004) The electronic structure of Mn in oxides, coordination complexes, and the oxygen-evolving complex of photosystem II studied by resonant inelastic scattering. J Am Chem Soc 126:9946–9959. doi:10.1021/ja038579z

Glatzel P, Yano J, Bergmann U, Visser H, Robblee JH, Gu W et al (2005) Resonant inelastic X-ray scattering (RIXS) spectroscopy at the Mn K absorption pre-edge—a direct probe of the 3d orbitals. J Phys Chem Solids 66(12):2163–2167. doi:10.1016/j.jpcs.2005.09.012

Greenwood NN, Earnshaw A (1984) Chemistry of the elements. Pergamon Press, Oxford, 1542 p

de Groot F (2001) XAFS theory and analysis of 3d transition metal compounds. Chem Rev 101:1779–1808. doi:10.1021/cr9900681

Guest CA, Schulze DG, Thompson IA, Huber DM (2002) Correlating manganese X-ray absorption near-edge structure spectra with extractable soil manganese. Soil Sci Soc Am J 66:1172–1181

Haskel D (1999) The FLUO package. http://www.aps.anl.gov/xfd/people/haskel

Heumann D, Dräger G, Bocharov S (1997) Angular-dependence in the K pre-edge XANES of cubic crystals: the separation of the empty metal e_g and $t_{2\ g}$ states of NiO and FeO. J Phys IV 7(C2):481–483

Jackson WE, Farges F, Yeager M, Mabrouk PA, Rossano S, Waychunas GA et al (2005) Spectroscopic study of Fe(II) in silicate glasses: implications for the coordination environment of Fe(II) in anhydrous silicate melts of geochemical interest. Geochim Cosmochim Acta 69:4315–4332. doi:10.1016/j.gca.2005.01.008

Kudo H, Miura H, Hariya Y (1990) Tetragonal monoclinic transformation of cryptomelane at high temperature. Min J 15:50–63. doi:10.2465/minerj.15.50

Lanson B, Drits VA, Gaillot A-C, Silvester E, Plançon A, Manceau A (2002) Structure of heavy-metal sorbed birnessite: part 1. Results from X-ray diffraction. Am Mineral 87:1631–1645

Manceau A, Llorca S, Calas G (1987) Crystal chemistry of cobalt and nickel in lithiophorite and asbolane from New Caledonia. Geochim Cosmochim Acta 51:105–113. doi:10.1016/0016-7037(87)90011-1

Manceau A, Gorshkov A, Drits V (1992a) Structural chemistry of Mn, Fe, Co and Ni in manganese hydrous oxides: part I. Information from XANES spectroscopy. Am Mineral 77:1133–1143

Manceau A, Gorshkov A, Drits V (1992b) Structural chemistry of Mn, Fe, Co and Ni in manganese hydrous oxides: Part II: Information from EXAFS spectroscopy and electron and X-ray diffraction. Am Mineral 77:1144–1157

Manceau A, Schlegel ML, Musso M, Sole VA, Gauthier C, Petit PE et al (2000) Crystal chemistry of trace elements in natural and synthetic goethite. Geochim Cosmochim Acta 64:3643–3661. doi:10.1016/S0016-7037(00)00427-0

Manceau A, Lanson B, Drits VA (2002) Structure of heavy metal sorbed birnessite. Part 3. Results from powder and polarized EXAFS spectroscopy. Geochim Cosmochim Acta 66:2639–2663. doi:10.1016/S0016-7037(02)00869-4

Manning PG (1970) Racah parameters and their relationships to lengths and covalencies of Mn^{2+} and Fe^{3+} oxygen bonds in silicates. Can Mineral 10:677–687

Manning PG (1973) Effect of second-nearest-neighbour interactions on Mn^{3+} absorption in pink and black tourmalines. Can Mineral 11:971–977

Marcus MA, Manceau A, Kersten M (2004) Mn, Fe, Zn and As speciation in a fast growing ferromanganese marine nodule. Geochim Cosmochim Acta 68:3125–3136. doi:10.1016/j.gca.2004.01.015

McKeown DA, Post JE (2001) Characterization of manganese oxide mineralogy in rock varnish and dendrites using X-ray absorption spectroscopy. Am Mineral 86:701–713

McKeown DA, Kot KK, Gan H, Pegg IL (2003) X-ray absorption studies of manganese valence and local environment in borosilicate waste glasses. J Non Cryst Solids 328:71–89. doi:10.1016/S0022-3093(03)00482-4

Nietubyc R, Sobczak E, Attenkofer KE (2001) X-ray absorption fine structure of manganese compounds. J Alloy Comp 328:126–131. doi:10.1016/S0925-8388(01)01332-9

Novak GA, Gibbs GV (1971) The crystal chemistry of the silicate garnets. Am Mineral 56:791–825

Oberti R, Hawtorne FC, Ungaretti L, Cannillo E (1993) A crystal chemical re-evaluation of amphibole/melt and amphibole/clinopyroxene DTi values in petrogenetic studies. Eur J Mineral 5:43–51

Pabst A (1943) Crystal structure of gillespite, $BaFeSi_4O_{10}$. Am Mineral 28:372–390

Papin A (2001) Etude expérimentale et spectroscopique de la cristallochimie du manganèse dans les silicates hydroxylés. Ph.D. thesis, Université d'Orléans, 191 p (in French; full text available at: http://tel.ccsd.cnrs.fr/documents/archives0/00/00/17/66/tel-00001766-00/tel-00001766.pdf)

Petrie LM (1999) Manganese. In: Marshall CP, Fairbridge RW (eds) Encyclopedia of geochemistry. Kluwer Academic, Dordrecht, pp 382–384

Post JE (1999) Manganese oxide minerals: crystal structures and economic and environmental significance. Proc Natl Acad Sci USA 96:3447–3454. doi:10.1073/pnas.96.7.3447

Post JE, Appleman DE (1994) Crystal structure refinement of lithiophorite. Am Mineral 79:370–374

Post JE, Bish DL (1988) Rietveld refinement of the todorokite structure. Am Mineral 73:861–869

Post JE, Veblen DR (1990) Crystal structure determination of synthetic sodium, magnesium, and potassium birnessite using TEM and the Rietveld method. Am Mineral 75:477–489

Post JE, Von Dreele RB, Buseck PR (1982) Symmetry and cation displacements in hollandites: structure refinements of hollandite, cryptomelane, and priderite. Acta Crystallogr B 38:1056–1065. doi:10.1107/S0567740882004968

Post JE, Heaney PJ, Hanson J (2003) Synchrotron X-ray diffraction study of the structure and dehydration behavior of todorokite. Am Mineral 88:142–150

Quartieri S, Triscari M, Sabatino G, Boscherini F, Sani A (2002) Fe and Mn K-edge XANES study of ancient Roman glasses. Eur J Mineral 14:749–756. doi:10.1127/0935-1221/2002/0014-0749

Reiche I, Chalmin E (2008) Synchrotron radiation and cultural heritage: combined XANES/XRF study at Mn K-edge of blue, grey or black coloured palaeontological and archaeological bone material. J Anal At Spectrom 23:799–806. doi:10.1039/b717442j

Reiche I, Vignaud C, Champagnon B, Panczer G, Brouder C, Morin G et al (2001) From mastodon ivory to gemstone: the origin of turquoise color in odontolite. Am Mineral 86:1519–1524

Ressler T, Wong J, Roos J, Smith JL (2000) Quantitative speciation of Mn-bearing particulates emitted from autos burning MMT-added gasolines using XANES spectroscopy. Environ Sci Technol 34:950–958. doi:10.1021/es990787x

Schulze DG, Sutton SR, Bajt S (1995) Determining manganese oxidation state using X-ray absorption near-edge structure (XANES) spectroscopy. Soil Sci Soc Am J 59:1540–1548

Shukla A, Calandra M, Taguchi M, Kotami A, Vankó G, Ccheong SW (2006) Polarized resonant inelastic X-ray scattering as an ultrafine probe of excited states of La2CuO4. Phys Rev Lett 96:077006. doi:10.1103/PhysRevLett.96.077006

Tebo BM, Bargar JR, Clement BG, Dick GJ, Murray KJ, Parker D et al (2004) Biogenic manganese oxides: properties and mechanisms of formation. Annu Rev Earth Planet Sci 32:287–328. doi:10.1146/annurev.earth.32.101802.120213

Tröger L, Arvanitis D, Baberschke K, Michaelis H, Grimm U, Zschech E (1992) Full correction of the self-absorption in soft-fluorescence extended X-ray absorption fine structure. Phys Rev B 46:3283–3289. doi:10.1103/PhysRevB.46.3283

Tromp M, Moulin J, Reid G, Evans J (2007) Cr K-Edge XANES spectroscopy: ligand and oxidation state dependence—what is oxidation state? AIP Conf Proc 882:699–701. doi:10.1063/1.2644637

Turner S, Buseck PR (1979) Manganese oxide tunnel structures and their intergrowths. Science 203:456–458 Medline. doi:10.1126/science.203.4379.456

Turner S, Buseck PR (1983) Defects in n'sutite (γ-MnO_2) and dry-cell battery efficiency. Nature 304:143–146. doi:10.1038/304143a0

Turner S, Post JE (1988) Refinement of the substructure and superstructure of romanechite. Am Mineral 73:1155–1161

Uozumi T, Kotani A, Parbelas JC (2004) Theory of $KL_{23}L_{23}$ Auger spectra around Ti-K pre-peaks of TiO_2. J Electron Spectrosc 137–140:623–627. doi:10.1016/j.elspec.2004.02.045

Visser H, Anxolabihhre-Mallart E, Bergmann U, Glatzel P, Robblee JH, Cramer SP et al (2001) Mn K-edge XANES and Kβ XES studies of two Mn-oxo binuclear complexes: investigation of three different oxidation states relevant to the oxygen evolving complex of photosystem II. J Am Chem Soc 123:7031–7039. doi:10.1021/ja004306h

Westre TE, Kennepohl P, DeWitt JG, Hedman B, Hodgson KO, Solomon EI (1997) A multiplet analysis of Fe K-edge 1 s → 3d pre-edge features of iron complexes. J Am Chem Soc 119:6297–6314. doi:10.1021/ja964352a

Wilke M, Farges F, Petit PE, Brown GE Jr, Martin F (2001) Oxidation state and coordination of Fe in minerals: an Fe *K* XANES spectroscopic study. Am Mineral 86:714–730

Winterer M (1997) XAFS—a data analysis program for materials science. J Phys IV 7(C2):243